Thin Solid Films 549 (2013) 216–223

Contents lists available at ScienceDirect

Thin Solid Films

journal homepage: www.elsevier.com/locate/tsf

Character and chemical-wear response of high alloy austenitic stainless steel (Ortron 90) surface engineered with magnetron sputtered Cr–B–N ternary alloy coatings

Bertram Mallia [a], Michael Stüber [b], Peter A. Dearnley [c,d,*]

[a] University of Malta, Department of Metallurgy and Materials Engineering, Msida, MSD 2080, Malta
[b] Karslruhe Institute of Technology (KIT), Karlsruhe, Germany
[c] nCATS, Engineering Sciences, University of Southampton, United Kingdom
[d] Boride Services Ltd, 6 Wynmore Drive, Leeds, LS16 9DQ, United Kingdom

ARTICLE INFO

Available online 5 September 2013

Keywords:
Cr–B–N coatings
Corrosion–wear
Tribo-corrosion
Chemical wear

ABSTRACT

Many transition metal borides, in particular CrB_2, show high inherent hardness, corrosion resistance and chemical stability. Appropriate additions of nitrogen to the Cr–B material system could in principle allow the synthesis of multi-phase materials containing hard, corrosion resistant (Cr–B, Cr–N) and lubricious (h-BN) phases providing a combination of good corrosion–wear resistance and in-situ lubrication. This factor has stimulated interest in the development of Cr–B–(N) magnetron sputtered thin tribological coatings. In the present reported work, several Cr–B–(N) coatings were produced by reactively sputtering a CrB_2 target in an argon atmosphere containing increasing amounts of nitrogen. They were mostly applied to Ortron 90 (Fe–20Cr–10Ni–2Mo–0.4N) austenitic stainless steel substrates. The coating structure changed from crystalline to largely amorphous with increasing nitrogen content, this was accompanied by a fall in nano-indentation hardness from 40 GPa at 0 at.% to 18 GPa at 21 at.%. N. The corrosion–wear performance of Cr–B–(N) coated Ortron 90 stainless steel when sliding against aluminium oxide in 0.9% saline solution, was worse than uncoated Ortron 90, due to their propensity to undergo chemical (dissolution) based wear. In these tests, no friction reduction was noted for the Cr–B–N coated materials. However, the $CrB_{1.87}$ coated Ortron 90 displayed superior corrosion–wear resistance and a slightly lower friction coefficient.

1. Introduction

Austenitic stainless steels are widely used in corrosion demanding applications due to their good corrosion resistance imparted by the stable chromium oxide passive layer. Despite their good general (static) corrosion resistance, such steels display poor degradation resistance when subjected to the conjoint (dynamic) actions of corrosion and wear, a phenomenon termed corrosion–wear [1]. Here, the protective passive film is broken down by mechanical contact, during sliding contact against other material surfaces. Accordingly, when used in sliding contacts in aqueous chloride ion containing fluids as found in nuclear, oil and gas and bio-medical devices, Ortron 90 (an Fe–20Cr–10Ni–2Mo–0.4N austenitic alloy) and related "super stainless steels" perform unsatisfactorily and may fail prematurely.

In principle, corrosion–wear performance of austenitic stainless steels can be improved with the application of hard, corrosion resistant layers through surface engineering techniques like magnetron sputter deposition [1,2]. Of the various coating materials, transition metal borides, particular those based on chromium have attracted a lot of interest, since they display both high hardness and very good corrosion resistance [3–7]. Moreover, it has been claimed that the minor addition of nitrogen (<30 at.%) to Cr–B coatings can result in the formation of the h-BN lubricous phase [8] which may serve as an in-situ lubricant, and lower the friction coefficient during use in sliding contact situations. It was the main aim of this study to test this hypothesis by subjecting a series of well characterised magnetron sputtered Cr–B and Cr–B–N coatings applied to Ortron 90 by subjecting them to reciprocating sliding contact tests against aluminium oxide whilst immersed in 0.89% NaCl solution at 37 °C.

2. Experimental procedure

2.1. Substrate preparation

The composition of the Ortron 90 austenitic stainless steel substrates used in this investigation is given in Table 1. This material was selected for the present work as it has long been used for sliding tribological contacts in saline environments due to its self-passivating nature which exceeds that of conventional 316L austenitic stainless steels and all ferritic steels, including hardened tool steels. Pieces of Orton

* Corresponding author at: Boride Services Ltd, 6 Wynmore Drive, Leeds, LS16 9DQ, United Kingdom. Tel.: +44 113 281 7634.
E-mail address: peter_dearnley@talktalk.net (P.A. Dearnley).

0040-6090/$ – see front matter © 2013 Elsevier B.V. All rights reserved.
http://dx.doi.org/10.1016/j.tsf.2013.08.093

Table 1
Chemical composition of Ortron 90 austenitic stainless steel substrates.

Material	Composition (wt.%)									
	Fe	Cr	Ni	Si	Mn	Nb	Mo	C	N	S
Orton 90	Bal.	20.7	9.66	0.35	3.91	0.32	2.17	0.04	0.39	<0.03

90, measuring 26 mm diameter and ~4 mm thick was ground to a 1200 grit finish using SiC abrasive (Struers MD-Piano 1200). This was followed by fine grinding using a 9 μm polycrystalline diamond and then polishing using a 3 μm polycrystalline diamond. The procedure achieved mirror finished substrates with an R_a and R_q of ~6 nm and 7 nm respectively.

2.2. Coating deposition

Cr–B–(N) coating deposition was carried out using a Leybold Z550 magnetron sputtering coating machine at the Institute for Applied Materials, Karlsruhe Institute of Technology, Germany. Mirror polished Ortron 90 stainless steel and cemented WC–Co (R_a better than 0.01 μm) were the substrate materials, the latter were used to enable a more rapid examination of the coatings via XRD and to obtain some cross-sectional fracture surfaces of the coatings. Following substrate cleaning in an argon atmosphere, an adhesion layer or "bond layer" of pure Cr was applied, followed by the boron enriched coatings. The latter were deposited from a 75 mm diameter hot pressed CrB_2 target (bonded to a PK75 copper backing plate) and were sputtered using a direct current power supply incorporating arc suppression control. Nitrogen content of the coatings was controlled by adding N_2 to the sputter chamber at specific flow rates. The sputter deposition conditions are summarised in Table 2. The substrates were stationary during deposition and no deliberate substrate heating was applied.

2.3. Basic coating characterisation

2.3.1. Coating microstructure, thickness, topography, chemical composition and crystallographic structure

The coating thickness was principally determined from polished coated Ortron 90 cross sections using a light optical microscope (LOM), whilst the grain morphology/microstructure of the coatings was determined from fracture cross sections on both WC–Co substrates and stainless steel. A Cameca Camebax Microbeam, electron probe micro-analysis (EPMA) wavelength dispersive X-ray analysis (WDX) system was used to determine the chemical composition for the Cr–B–(N) coatings. This dedicated microprobe technique has excellent capability for analysing light elements like boron and nitrogen in heavy element matrices, being far superior to those attainable using the more popular EDX (energy dispersive X-ray analysis) method attached to standard SEMs. Mirror finished Cr–B–(N) coated Ortron 90 were used for the analysis. The topography of the coated and uncoated Ortron 90 was investigated using a field emission scanning electron microscope (FEGSEM), 3D-WyKo interferometer and 2D-Talysurf profilometer. The coating structure was investigated using a Seiffert C3000 X-ray diffractometer. X-ray diffraction was carried out using Cu-Kα radiation and a θ–2θ geometry. Cr–B–(N) coated Ortron 90 and WC–Co substrates were scanned between 20 and 90° of 2 theta using a step size of 0.05° and a scan rate of 0.01°/s.

Table 2
Deposition parameters for the Cr–B–(N) deposition runs.

		Coating identification			
		C0	C1	C2	C3
Substrate sputter cleaning conditions	Forward r.f. power (W)	500	500	500	500
	Chamber pressure (Pa)	0.6	0.6	0.6	0.6
	Duration (min)	15	15	15	15
	Chamber atmosphere	Ar	Ar	Ar	Ar
Coating deposition conditions	CrB_2 target d.c. sputtering power (W)	250	250	250	250
	Chamber pressure (Pa)	0.6	0.6	0.6	0.6
	Chamber atmosphere	Ar	Ar + N	Ar + N	Ar + N
	N_2 flow (sccm)	0	1	5	10
	Induced substrate bias	Grounded	Grounded	Grounded	Grounded
	Deposition time (min)	90	90	90	90

2.3.2. Mechanical properties

Nanohardness testing was conducted on the coated samples using a Nano Test system from Micromaterials, Wrexham, UK. A Berkovich diamond indenter was fitted for all tests. The equipment was calibrated against a fused silica standard prior to sample testing. Depth versus load hysteresis testing was undertaken in depth controlled (200 nm) mode. The loading and unloading rates were 3 mN/s with a dwell period of 30 s at maximum load. For each material a nano-indentation array of 20 indentations was made. The raw data was analysed using a software provided by the equipment manufacturer (Micromaterials) that uses a power law fit (Oliver and Pharr fit) to determine the plastic depth and extract the mechanical properties of the coating.

To qualitatively asses the coated Ortron 90 test-piece responses to larger scale mechanical deformation, a series of Rockwell C indentations were performed using an Indentec 8187.5 LKV universal hardness testing machine. The damage caused, around the indentation rims, was recorded using light optical microphotography.

2.4. Static corrosion tests

A computer driven potentiostat (EG&G Versastat II model K0235) in conjunction with an EG&G PARC three electrode flat cell, was used to study the open circuit potential (OCP) and single cycle voltammetry (CV) behaviour of the coated and uncoated test pieces. All electrochemical tests were carried out at 37 ± 1 °C in nitrogen de-aerated 0.9 wt.% NaCl solution, whereby a sample surface area of 1 cm^2 was exposed to the electrolyte. The reference electrode was Ag/AgCl and the counter electrode was high purity Pt. The open circuit potential was measured just after the sample made contact with the electrolyte and was monitored for 1 h. Subsequently the sample was polarized for 10 min at −1.0 V Ag/AgCl and a single cycle CV test was then made at a scan rate of 0.167 mV/s. The scan reversal was performed at 1 mA. After testing the samples were gently immersed in distilled water to avoid salt crystal precipitation.

2.5. Dynamic sliding contact corrosion–wear tests

Fig. 1 shows the test rig used to assess the reciprocation sliding contact corrosion–wear behaviour of Cr–B–(N) coated and uncoated Ortron 90. Each test specimen was tightly secured to the test platform using a conducting copper screw (Fig. 1) connected to the potentiostat. The 0.9% NaCl test electrolyte was heated to and maintained at 37 ± 1 °C via a heated water jacket. A 7.94 mm diameter sintered poly-crystalline α-Al_2O_3 ball was used as the counterface material. The latter material was selected to avoid adverse current generation resulting from galvanic coupling effects. Once the electrolyte was at temperature, the open circuit potential (OCP) of the test specimen with respect to a Ag/AgCl reference electrode was measured for ~10 min. A load of 200 g was then applied to the test samples via the loading arm acting on the α-Al_2O_3 ball. For the uncoated Ortron

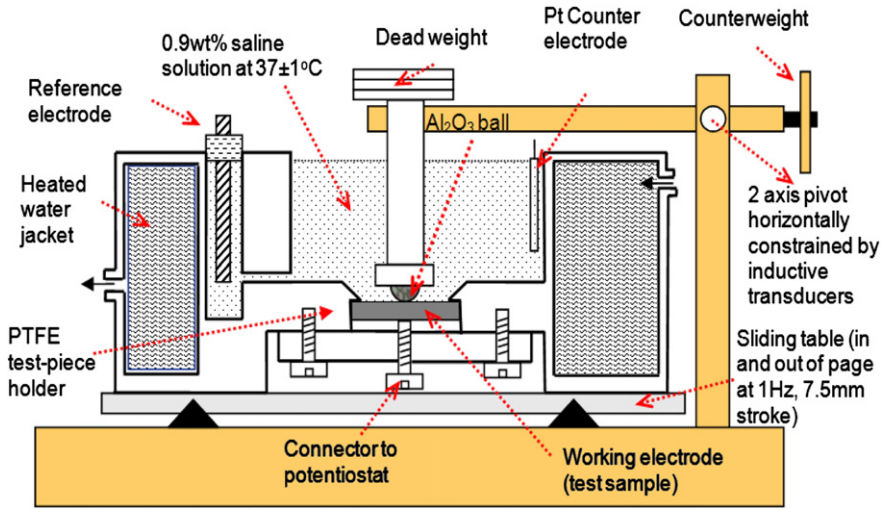

Fig. 1. Schematic representation of corrosion–wear set-up.

Table 3
Chemical composition determined by WDX for Cr–B–(N) coated Ortron 90.

Coating identification	Chemical composition (at%)				B/Cr ratio
	N	B	Cr	Ar	
C0	0	64.85	34.75	0.03	1.87
C1	3.83	61.82	33.84	0.13	1.83
C2	11.52	57.01	30.94	0.22	1.84
C3	21.45	49.8	28.24	0.2	1.76

90 test-piece this equated to an initial subsurface shear stress of ~204 MPa that was ~42% of the substrate shear yield strength based on its Vickers microhardness of 341 kg/mm^2. All tests were carried out at a frequency of 1 Hz, over a test track length of 7.5 mm for 7200 s (2 h). During testing the dynamic OCP and frictional force were measured simultaneously via a data acquisition card connected to a PC that ran a dedicated Labview program. At the end of each corrosion–wear test the OCP was monitored for a further 5 min. All corrosion–wear tests were repeated three times.

A non-contacting light optical (Wyko) surface profilometer technique was used to determine the cross sectional area (μm^2) of the corrosion–wear tracks of the uncoated and Cr–B–(N) coated Ortron 90. This was determined at three different positions along each test track and the average value determined. This figure was then multiplied by 1 to give the total material loss (TML) value in μm^3.

2.6. Inductively coupled plasma (ICP) analysis of used electrolyte

An Elan DRC-e, ICP-MS (mass spectrometer) system was used to quantitatively determine the solutionised ion contents of the test electrolytes (after completion of the corrosion–wear tests). The ICP-MS technique has the ability to effectively generate single charge of ions from the elemental species within a sample. The ions are directed into a mass spectrometer and separated according to their ion-to-mass ratio. The equipment was calibrated on standards in the concentration range of 1 to 100 ppb for the elements being investigated here. The detection limits were in the parts per trillion range.

3. Results

3.1. Coating microstructure, composition, surface appearance, roughness, hardness and thickness

The chemical composition of magnetron sputtered Cr–B–(N) coatings applied to Ortron 90 is given in Table 3. The coatings had a B/Cr ratio ranging from 1.76 to 1.87 which decreased with increasing nitrogen content. Argon incorporation in most cases was less than 0.3 at.%.

The Cr–B–(N) coatings were ~5 μm thick (Table 4) and their surface roughness (Table 4) increased compared to the mirror polished Ortron 90 substrate. Surface imaging revealed plenty of small and randomly oriented hemispherical asperities ranging from submicrometer to ~3 μm diameter (Fig. 2) and occasional overgrowth defects or depressions in the coating as revealed by 3D surface profilometry. Cross-sectional fracture surfaces through the coatings and adjacent substrates revealed no clear grain morphology in the coatings. The Cr–64.8B (C0) coating showed a slightly rougher fracture surface (Fig. 3a) compared to those coatings containing N, as for example shown for the Cr–B–21.4N coated Ortron 90 (C3), Fig. 3b. For the latter, it was also possible to see the intermediate "bond" layer of Cr between the substrate and the coating (Fig. 3b). No clear coating grain structure was visible from the fracture surfaces and there was no obvious evidence of micro-porosity.

The extent of coating crystallinity was evident from the XRD results (Fig. 4). These showed the basic Cr–64.8B coating (C0) to be crystalline with a hexagonal 101 preferred orientation whilst the Scherrer grain size, determined from the width of the 101 peak was ~13.5 nm.

Table 4
Thickness, surface roughness, microhardness, nanohardness and reduced modulus values for Cr–B–(N) coated and uncoated Ortron 90.

Sample designation	Thickness (μm)	Surface roughness (μm)		Micro-hardness (HV/0.05)	Nano-hardness to 200 nm depth (GPa)	Reduced modulus (GPa)
		R_a	R_q			
Uncoated Ortron 90	/	0.0060	0.0070	341	/	/
C0 Cr–64.8B coated	4.6	0.0137	0.0363	2565	40.6	360.1
C1 Cr–B–3.8N coated	4.9	0.0076	0.0124	1940	28.8	322.3
C2 Cr–B–11.5N coated	5.1	0.0100	0.0158	1613	22.1	282.8
C3 Cr–B–21.4N coated	5.5	0.0109	0.0225	1292	18.4	228.7

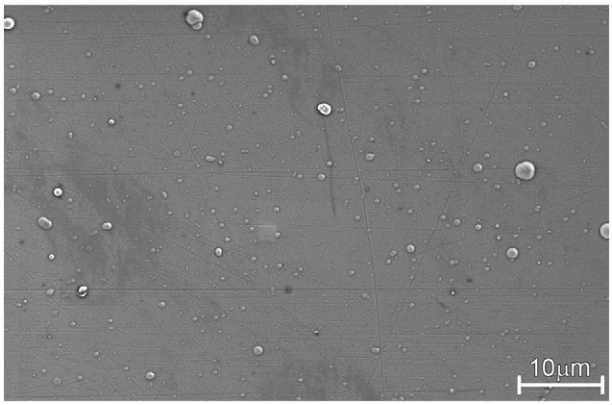

Fig. 2. Topography of a Cr–B–3.8N coated (C1) Ortron 90 test-piece (FEGSEM).

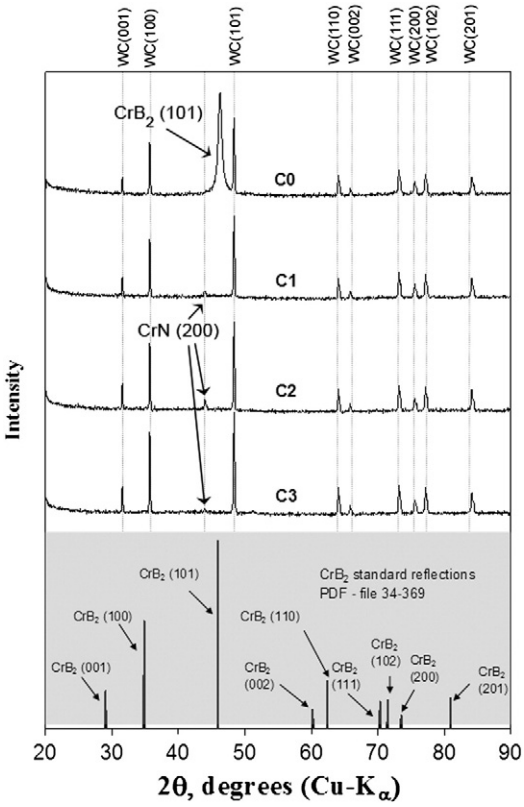

Fig. 4. XRD patterns obtained for Cr–B–(N) coated WC–Co variants. Refer to Table 3 for coating compositions.

The addition of nitrogen to the basic Cr–B coating (C1, C2, C3) resulted in largely amorphous coatings — the CrB_2 101 diffraction peak disappeared and only low intensity cubic crystalline CrN 200 reflections (ICDD 11-0065; see Fig. 4), could be detected. No crystalline B containing phases could be detected.

Microhardness and nano-indentation hardness results showed that crystalline Cr–64.8B (C0) to be very hard (2565 kg/mm^2 and 40 GPa respectively — Table 4) with a reduced modulus of ~350 GPa. The effect of introducing N_2 into the sputter deposition process was to create Cr–B–N coatings with lower hardness and reduced modulus, which decreased with increasing N content (Table 4). The change in hardness with respect to increasing nitrogen content agrees with the earlier findings of Budna et al. [8].

The adhesion and resistance to failure of the Cr–B–(N) coatings were investigated by Rockwell C indentations. C0 was brittle but adherent to the substrate as indicated by the resistance against delamination around the indentation rims (Fig. 5). Brittleness was displayed by a high density of radial cracks coupled with transverse cracking (Fig. 5a). Coatings C1 to C3 displayed similar radial cracking but without transverse cracking (Fig. 5b), indicating the Cr–B–N coated materials to be more fracture resistant compared to CrB_2 coated Ortron 90.

3.2. Static corrosion tests

Examples of cyclic polarization (CP) plots for Cr–B–(N) coated and uncoated Ortron 90 are shown in Fig. 6. Examination of the CP tested coated and uncoated Ortron 90 surfaces showed that crevice corrosion (beneath the gasket seal on the flat cell) was only significant for the uncoated substrate. Here, the crevices were ~6 μm deep and 0.2 mm wide. No pitting corrosion was observed. Conversely only slight crevice corrosion (<0.1 μm deep) was observed for the Cr–B–(N) coated Ortron 90 variants and there was no significant pitting of the main test surface due to corrosion. However, LOM observations of the coated surfaces after CP tests revealed a multi-coloured (various shades of red and blue) corrosion film that was ~200 nm thick, indicative of uniform corrosion. SEM-EDX analysis demonstrated the films to be enriched in oxygen and chromium. Film formation was not observed on the uncoated Ortron 90. The higher break-down potential of the latter material (see the change in slope at around 1.2 V — Fig. 6) was attributed to the onset of crevice corrosion. In contrast, the lower break-down potential of all the coated Ortron 90 materials (see the change in slope at around 0.7 V — Fig. 6) indicates the onset of the uniform corrosion was energetically easier compared to the pitting corrosion of the uncoated material, so ion solution would be slightly easier for the coated materials compared to the uncoated variant.

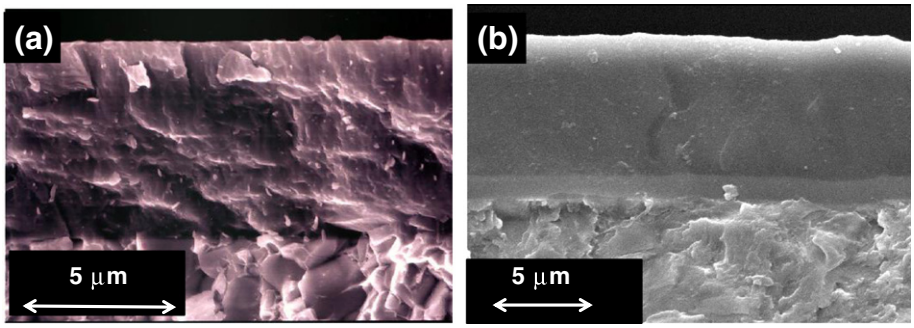

Fig. 3. SEM images of fracture surfaces showing (a) CrB2 coated WC–Co (Ref C0) and (b) Cr–B–N coated stainless steel (Ref C3).

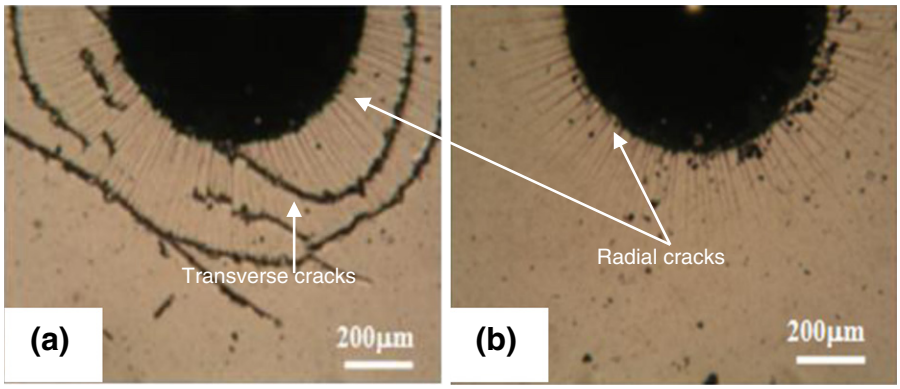

Fig. 5. Light optical micrographs of Rockwell C indentations made on: (a) Cr–64.8B coated (C0) coated and (b) Cr–B–11.5N coated (C2) Ortron 90 test-pieces.

3.3. Sliding contact corrosion–wear tests

3.3.1. Dynamic friction and OCP measurements

Examples of the real time dynamic friction (μ) and open circuit potential (OCP) outputs recorded throughout the sliding contact tests, are shown in Fig. 7, whilst the dynamic friction coefficients and total material losses for all the test materials are collated in Table 5. It should be noted that none of the Cr–B–(N) coatings were penetrated during the tests. The dynamic μ during the test on Cr–64.8B coated Ortron 90 (C0) was lowest of all (~0.37) compared to intermediate values observed for uncoated Ortron 90 (~0.44) and the much higher values for the N containing coatings, C1, C2 and C3 (~0.56) — see Fig. 7. This is in general agreement with the findings of Budna et al. [8] for the non-lubricated (dry) sliding of Al_2O_3 against Cr–B–N coated high speed tool steels in laboratory air, where high friction values > 0.6 were observed — no friction lowering being evident.

3.3.2. Corrosion–wear material losses and test track morphologies

The average total material loss values obtained from the corrosion–wear tracks produced on the coated and uncoated Ortron 90 are collated in Table 5. The C0 coated Ortron90 displayed the smallest material loss followed by uncoated Ortron 90, but material losses were significantly higher for the Cr–B–N coated materials.

FEGSEM examinations of the corrosion–wear tracks on the uncoated Ortron 90 test material revealed numerous (but very thin, <0.1 μm deep) plastic deformation bands oriented in the direction of sliding contact. Deformation action also yielded debris with a fine plate like morphology (Fig. 8a). Unfiltered 2D Wyko profilometry across the uncoated Ortron 90 corrosion–wear tracks showed a series of troughs having a depth ranging from ~0.4 to 1 μm. In contrast, however, the corrosion–wear tracks formed on the Cr–B–(N) coatings were observed to be very smooth (confirmed by 2D Wyko profilometry) and featureless with no evidence of localised plastic deformation (Fig. 8b). The coatings had been gradually worn down, but not removed completely, and there was no evidence of coating fracture or coating loss by pull-out. In the case of the more wear resistant C0 coatings a series of parallel troughs (~0.3 to 0.5 μm deep) oriented in the direction of sliding contact were evident.

3.3.3. Morphology of debris

FEGSEM examinations revealed debris along the edges of all the corrosion–wear test tracks (Fig. 8c). This could be present as fine individual particles (~50 nm across) but more typically comprised agglomerates of particles (between 0.5 and 10 μm in diameter). Some debris displayed smooth, flat morphologies whilst others could be rougher (Fig. 8c).

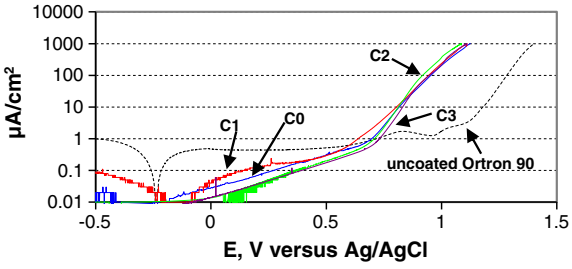

Fig. 6. Cyclic voltammetry (CP) plots (reverse sweep data removed for clarity) for Cr–B–(N) coated and uncoated Ortron 90. Refer to Table 3 for coating compositions.

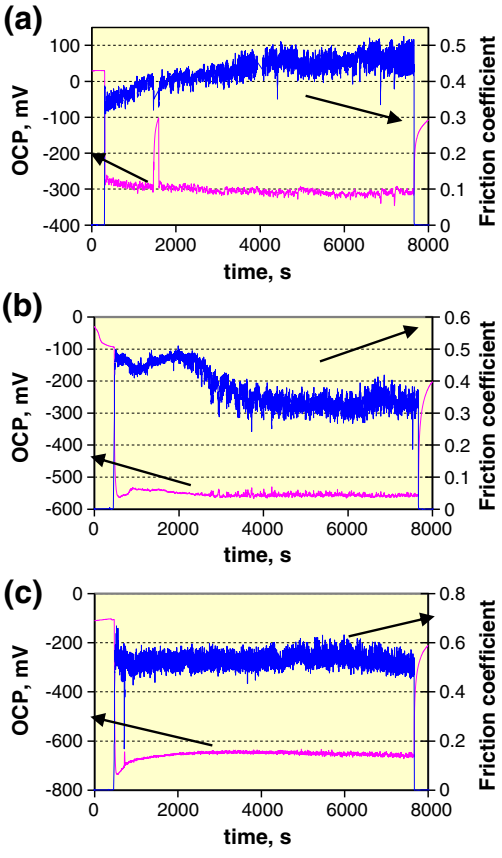

Fig. 7. Real time OCP and μ data collected during corrosion wear testing. Al_2O_3 balls were made to slide against (a) uncoated Ortron 90; (b) Cr–64.8B coated Ortron 90 (C0) and (c) C3 coated Ortron 90. The initial sharp rise in friction (in all tests) corresponds to the onset of the sliding contact. Refer to Table 3 for coating compositions.

Table 5
Corrosion–wear data for Cr–B–(N) coated and uncoated Ortron 90.

Specimen designation	Track roughness[a] (μm)			Total material loss (TML) volume (μm³) determined via 2D profilometry	Average dynamic friction coefficient (μ) sliding against an Al_2O_3 ball
	R_a	R_q	R_t		
Ortron 90	0.10	0.15	1.05	418 ± 19	0.44 ± 0.007
C0	0.11	0.14	0.75.	338 ± 36	0.46 ± 0.007[b]; 0.37 ± 0.007[c]
C1	0.05	0.06	0.32	573 ± 78	0.52 ± 0.007[b]; 0.42 ± 0.007[c]
C2	0.07	0.10	0.41	1071 ± 170	0.57 ± 0.007
C3	0.05	0.07	0.36	804 ± 17	0.55 ± 0.021

[a] Track roughness was taken in a direction perpendicular to sliding direction.
[b] Average dynamic μ before transition to a lower value.
[c] Average dynamic μ after transition to a lower value.

3.3.4. Examination of the Al_2O_3 counterface contact surfaces

All of the Al_2O_3 ball contact surfaces exhibited very little material loss, regardless of whether sliding against the coated or uncoated Ortron 90 test-pieces. Transfer layers of varying thicknesses (determined to be ~0.2 to 1.0 μm using 2D Wyko Profilometry) were frequently detected on the used ball surfaces, ranging in smoothness and morphology, Fig. 9. Sometimes the transfer layer was cracked. Parts of the Al_2O_3 ball contact surfaces (with no transfer layer coverage) were generally smooth with no evidence of grain pull-out, Fig. 9.

3.3.5. Used electrolyte analysis

Following the sliding corrosion–wear tests, the Fe, Cr and B ion concentrations were determined in the test solution. The Fe ion concentration was ~2 ppb for tests made against uncoated Ortron 90, whereas, Fe was not detected in test solutions used for corrosion–wear testing against the Cr–B–(N) coated Ortron 90 variants. The Cr ion concentration detected in the test solutions for the coated and uncoated Ortron 90 were very small (<5 ppb), whereas, the B ion concentration for test solutions against Cr–B–(N) coated Ortron 90 is between 50 and 100 ppb (parts per billion) and were highest (>60 ppb) in the electrolytes used to test Ortron 90 coated with variants containing N, Fig. 10.

4. Discussion

4.1. Character of the coatings

The C0 coating had the composition Cr–64.8B (Table 3) and a B:Cr ratio of 1.87 equating to a formula of $CrB_{1.87}$ rather than the stoichiometric CrB_2. The same phenomenon of boron depletion has also been reported by Zhou et al. [9] and can be attributed to the scattering of the sputtered boron target ions within the argon plasma or to preferential re-sputtering of the coating on the substrate. Introducing a partial pressure of N_2 into the Ar plasma, results in the incorporation of this element into the coatings, as shown Table 3 (coatings C1, C2 and C3).

According to the equilibrium ternary phase diagram [10], the single CrB_2 phase field moves to ternary Cr_xB_y + Cr_xN + BN phase field with the addition of nitrogen. The Gibbs free energies for the formation of BN, Cr_2N, CrN, CrB and CrB_2 are −228.5, −102.2, −92.7, −77.0 and −95.2 KJ/mol respectively [11], so the driving force for the formation of BN > Cr_2N > CrN. This is general agreement with the earliest research dealing with the destabilisation of CrB_2 by N at elevated temperature, reported in 1966 [12] where the decomposition products of BN and CrN were detected. XRD showed that those coatings produced in the present work (Fig. 4) which incorporated nitrogen (C1, C2 and C3) contained no detectable crystalline Cr–B phases, particularly CrB_2 nor CrB. Instead most of these coatings were almost completely non-crystalline with only substrate diffraction peaks being observed — this indicates that the X-rays completely penetrated the coatings during XRD. However, there was some evidence for very small quantities of crystalline CrN (Fig. 4) in coatings C1, C2 and C3. This is in agreement with the transmission electron microscopy and XRD evidence reported by Budna et al. [8], Lin et al. [13], Gorishnyy et al. [14] and Hegedus et al. [15] who consider that such coatings essentially comprise an amorphous Cr–B–N matrix containing small crystalline regions of CrN and non-crystalline (amorphous) BN, although unequivocal evidence of the latter phase has not been established. Nonetheless, it is clear from the results reported here and from those cited by others that only a small quantity of interstitial N (<4 at.%) is needed to destabilise the formation of CrB_2 during reactive sputtering.

Coating Cr–64.8B (C0) attained the highest nano-indentation hardness (~40 GPa) which is in agreement with previously published reports [4,13]. This can be attributed to the strong covalent bonding within CrB_2 (characterised by its high melting temperature ~2200 °C) and the very fine grain size of the coatings (measured via the X-ray Scherrer technique [16]). Here the large grain boundary area inhibits deformation between grains. The addition of nitrogen to the basic $CrB_{1.9}$ coating decreased the magnitude of both the nano-indentation hardness and the reduced modulus (Table 4). The possible formation of amorphous BN (reported by others [8,13–15]) may have contributed to this effect but the lack of long range ordering (non-crystallinity) revealed by XRD (Fig. 4) suggests a more open atomic arrangement of atoms in the Cr–B–N coatings with substantially fewer co-valent bonds. This may also explain the reduction in the amount of fracture

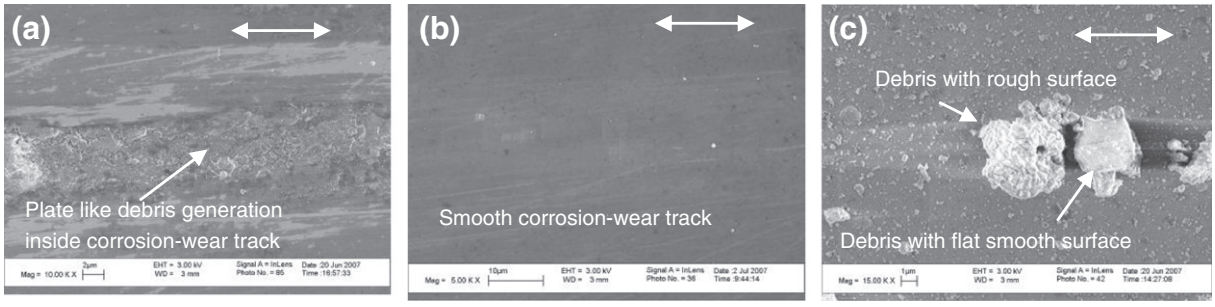

Fig. 8. FEGSEM images showing details of the test surfaces after corrosion–wear testing (sliding against Al_2O_3 in 0.9 wt.% NaCl): (a) uncoated Ortron 90 and (b) C3 coated Ortron 90 and; (c) Debris on C0 coated Ortron 90. The double headed arrows indicate the directions of reciprocation sliding during the tests.

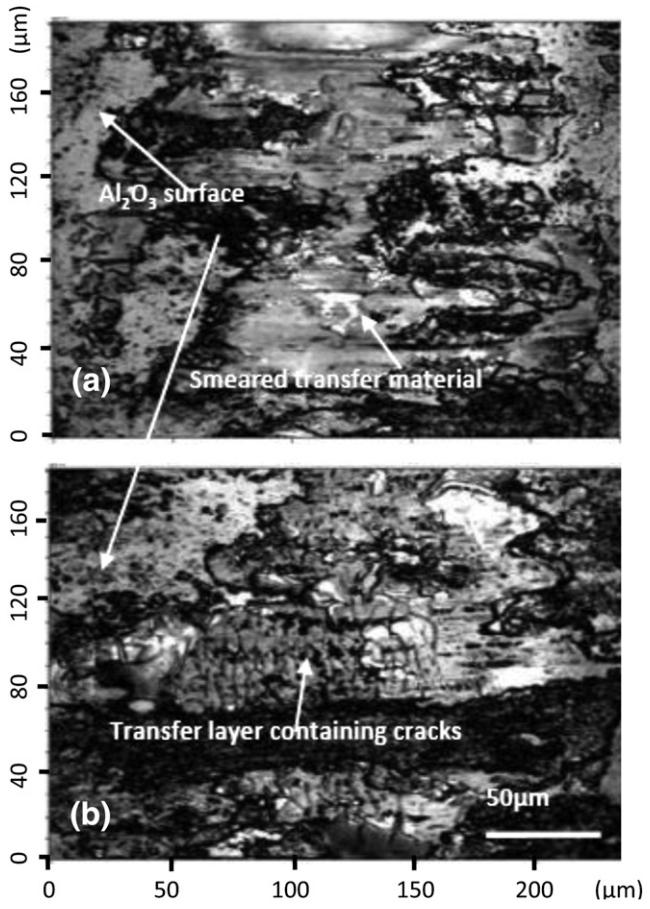

Fig. 9. Wyko instrument images of Al_2O_3 ball contact surfaces after testing against (a) C0 and (b) C3 coated Ortron 90. Refer to Table 3 for coating compositions.

observed after Rockwell C indentation (Fig. 5). Accordingly, these materials were slightly tougher (fracture resistant) than the Cr–64.8B (C0) coatings.

4.2. Corrosion–wear of uncoated and coated Ortron 90 stainless steel

In order to explain the corrosion–wear results in a logical manner we propose the hypothesis that the smoothly degraded corrosion–wear track surfaces observed for the Cr–B–N coated Ortron 90 test-pieces (Fig. 8b) were caused by a chemical wear process, whereby the coating material became dissolved in the electrolyte. In support of this argument is the observation that the B ion content of the used 0.89% NaCl electrolyte (analysed by the ICP-MS technique after corrosion–wear testing) was proportional to the corrosion–wear test track cross-sectional area (see Fig. 10). Conversely the Cr ion levels were very much lower and of a very similar value irrespective of the type of coated test-piece. Hence, little, if any, dissolution of the Cr took place. The precise nature of the dissolution of the B or possibly amorphous BN by the saline test solution is not clear without a deeper and more elaborate investigation procedure. It is possible that direct and continuous dissolution took place, or that a passive film was initially formed, that became repeatedly damaged and removed by mechanical contact, in the manner proposed for other coated materials tested in a similar manner. This latter process has been termed Type I corrosion–wear [1,2]. Mechanical material loss, due to plastic shearing of micro-asperities, is another feasible mechanism observed in other work [1]. Based on the examination of the uncoated Ortron 90 test tracks (Fig. 8a) this appears probable, but it is noted that the comparative low strength and nano-indentation hardness (Table 4) of the uncoated material resulted in only a slightly higher rate of corrosion–wear compared to the very much harder $CrB_{1.87}$ coated

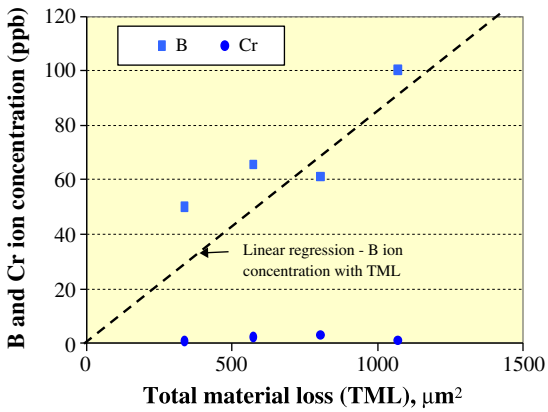

Fig. 10. B and Cr ion concentrations detected in the used test electrolytes (via the ICP-MS technique) after corrosion–wear testing of Cr–B–(N)-coated Ortron 90 test pieces.

material. Accordingly, mechanical stimulated dissolution based degradation of the uncoated material cannot be ruled out. Similarly, a moderate amount of B solution was observed for the $CrB_{1.87}$ coated material (left-most data point in Fig. 10), suggesting some dissolution driven wear for this material as well.

It is clear from the above that fracture toughness (resistance to fracture growth), hardness/yield strength and the elastic modulus properties often invoked to explain the degradation of materials through wear was not of major importance to the durability of the test-materials subjected to corrosion–wear testing herein. There was no evidence to support the idea that any form of coating loss via micro-fracture/tearing or pull-out took place, since only very smooth wear surfaces of the Cr–B–N coated materials were observed (Section 3.3.2) and the coatings were never completely worn through to their substrates.

It is also apparent that BN, even if present (as an amorphous phase) in any of the coatings, provided no benefit to coating durability. Most notably, the dynamic friction coefficient was higher for the Cr–B–N coated materials compared to the uncoated and $CrB_{1.87}$ coated material (Table 5). Hence, the Cr–B–N coating materials did not show any friction lowering capability which agrees with the findings of Budna et al. [8], who studied the dry friction behaviour between α-Al_2O_3 and various Cr–B–N coated high speed steels.

5. Conclusions

A series of Cr–B–(N) coatings (~5 μm thick) were successfully applied to a series of Ortron 90 (an Fe–20Cr–10Ni–2Mo–0.4N austenitic alloy) and WC–Co substrates via direct current (d.c.) magnetron sputtering. They had the following characteristics:

1. Coatings prepared by sputtering of a hot pressed stoichiometric CrB_2 target disc with a 100% Ar plasma were crystalline having the nominal formula Cr–64.8B (C0) coatings that equated to a sub-stoichiometric composition of $CrB_{1.87}$.
2. Coatings prepared by sputtering of a hot pressed stoichiometric CrB_2 target disc with an Ar plasma containing different levels of N_2 allowed a range of Cr–B–N coatings with differing nitrogen contents ranging from 4 to 21 at.% to be synthesised. All Cr–B–N type coatings were essentially amorphous although XRD indicated that they contained very small amounts of crystalline CrN. No crystalline BN was detected, but work reported by others suggest amorphous BN might have been contained within the Cr–B–N coatings.
3. Rockwell C indentation testing of the amorphous Cr–B–N coated Ortron 90 test-pieces, revealed them to be slightly tougher (more fracture resistant) compared to the crystalline Cr–64.8B ($CrB_{1.87}$) coated Ortron 90 materials. The addition of interstitial nitrogen had

the effect of markedly reducing nano-indentation hardness from ~40 GPa for the Cr–64.8B coating to 29, 22 and 18 GPa for Cr–B–4N, Cr–B–11N and Cr–B–21N respectively.

4. Static single cycle polarization corrosion tests showed the Cr–B–(N) coated Ortron 90 test-pieces to be resistant to pitting and crevice corrosion in saline solution but displayed a lower breakdown potential compared to uncoated Ortron 90. The latter material displayed crevice corrosion via pitting during passive film break down.

The following conclusions are based on a series of reciprocating (1 Hz) sliding corrosion–wear tests conducted in 0.9% NaCl electrolyte solution at 37 °C where an Al_2O_3 ball was used to apply an initial contact pressure of ~660 MPa to Cr–B–(N) coated and uncoated Ortron 90 test piece surfaces.

A. Only the $CrB_{1.87}$ coated Ortron 90 displayed better corrosion–wear resistance than uncoated Ortron 90.
B. All coatings containing N were less corrosion wear resistant than uncoated Ortron 90.
C. Material loss during the sliding contact tests, was hypothesized to be due to chemical type wear processes, typically rendering the test track surfaces smooth when examined by FEGSEM. This process may have been the result of direct material dissolution or via the intermittent mechanical removal of protective passive films, previously reported as the Type I corrosion–wear mechanism.
D. Chemical type wear processes dominated the degradation of the Cr–B–N coated materials, whilst they probably also contributed in part to the lower degradation rates of the uncoated and $CrB_{1.87}$ coated materials.
E. A contribution to the total material loss of the uncoated Ortron 90 resulted from mechanical wear caused by micro-asperity shearing.
F. The magnitude of mechanical properties alone, like the fracture toughness (resistance to fracture growth), hardness/yield strength and the elastic modulus often invoked to explain material loss through wear were not considered to be of major importance to the durability of the test-materials when subjected to sliding contact tests in 0.89% NaCl solution.
G. The Cr–B–N based coating materials did not lower friction during corrosion–wear testing. On the contrary, higher friction coefficients were observed compared to the uncoated and $CrB_{1.87}$ coated Ortron 90 test-pieces.

References

[1] P.A. Dearnley, B. Mallia, Wear 306 (2013) 263.
[2] P.A. Dearnley, G. Aldrich-Smith, Wear 256 (2004) 491.
[3] M. Audronis, P.J. Kelly, A. Leyland, A. Matthews, Thin Solid Films 515 (2006) 1511.
[4] K.L. Dahm, L.R. Jordan, J. Haase, P.A. Dearnley, Surf. Coat. Technol. 108–109 (1998) 413.
[5] T.P. Moffat, R.M. Latanision, J. Electrochem. Soc. 138 (1991) 3280.
[6] R.R. Ruf, C.C. Tsuei, J. Appl. Phys. 54 (1983) 5705.
[7] P. Schwarzkopf, R. Kieffer, Refractory Hard Metals, The Macmillan Company, New York, 1953.
[8] K.P. Budna, P.H. Mayrhofer, J. Neidhardt, E. Hegedus, I. Kovacs, L. Toth, B. Pecz, C. Mitterer, Surf. Coat. Technol. 202 (2008) 3088.
[9] M. Zhou, M. Nose, Y. Makino, K. Nogi, Thin Solid Films 359 (2000) 165.
[10] P. Rogl, J. Schuster, Phase Diagrams of Ternary Boron Nitride and Silicon Nitride Systems, ASM, Materials Park Ohio, 1992.
[11] I. Barin, Thermochemical Data for Pure Substances, Third ed. Weinheim, New York, 1995.
[12] H.J. Goldschmidt, Interstitial Alloys, Butterworths, London, 1966. 572.
[13] J. Lin, J.J. Moore, W.C. Moerbe, M. Pinkas, B. Mishra, G.L. Doll, Int. J. Refract. Met. Hard Mater. 28 (2010) 2.
[14] T.Z. Gorishnyy, D. Mihut, S.L. Rohd, S.M. Aouadi, Thin Solid Films 445 (2003) 96.
[15] E. Hegedus, I. Kovacs, B. Pecza, L. Toth, K.P. Budnab, C. Mitterer, Vacuum 82 (2008) 209.
[16] B. Mallia, PhD Thesis, University of Leeds (UK), 2008.